Electronic Supplementary Material (ESI) for Journal of Materials Chemistry C.

Electronic Supplementary Information

Room Temperature Perylene Based Columnar Liquid Crystals as Solid-State Fluorescent Emitters in Solution-Processable Organic Light-Emitting Diodes

Indu Bala,[a] Nitya Singh,[a] Rohit Ashok Kumar Yadav,[b] Joydip De,[a] Santosh Prasad Gupta,[c] Dharmendra Pratap Singh,[d] Deepak Kumar Dubey,[b] Jwo-Huei Jou[b], Redouane Douali[d] and Santanu Kumar Pal*[a]

---

[a]*Department of Chemical Sciences, Indian Institute of Science Education and Research (IISER) Mohali, Sector-81, SAS Nagar, Knowledge City, Manauli-140306, India. E-mail:* skpal@iisermohali.ac.in, santanupal.20@gmail.com
[b]*Department of Materials Science and Engineering, National Tsing Hua University, Hsinchu 30013, Taiwan*
[c]*Department of Physics, Patna University, Patna- 800005*
[d]*Unité de Dynamique et Structure des Matériaux Moléculaires (UDSMM), Université du Littoral Côte d'Opale (ULCO), 50 Rue Ferdinand Buisson, 62228, Calais, France*

Table of Contents:

1. Experimental Section

1.1 Materials and reagents: The commercially available chemicals were used as such. 3,4,9,10-perylenetetracarboxylic dianhydride was bought from TCI chemicals. Potassium hydroxide (KOH), tetraoctylammoniumbromide (TOAB), propargyl bromide, 1-Bromo-3,7-dimethyloctane, 1-bromohexane, 1-bromooctane, 1-bromodecane, Copper sulphate ($CuSO_4$), sodium ascorbate, sodium azide (NaN_3) were all purchased from Sigma-Aldrich. The solvents: dimethysulfoxide (DMSO), ethanol (EtOH), chloroform ($CHCl_3$) used in synthesis were bought from Merck. Distilled water has been used to perform reactions wherever is needed. Lithium fluoride (LiF), aluminium (Al) and indium tin oxide (ITO) were used during fabrication in OLED devices. Silica gel (60-120) and neutral alumina gel were used to purify the intermediates and target materials by column chromatographic techniques. Thin-layer chromatography (TLC) was performed on alumina sheets pre-coated with silica gel (Merck, Kieselgel 60, F254).

1.2 Instrumentation: The detailed specifications of instruments used for structural characterization (NMR, Mass, FT-IR), thermal characterization (Microscopy, Thermal gravimetric analysis (TGA), Differential scanning calorimetry (DSC), X-Ray diffraction (XRD)), photophysical studies (UV-Vis & Fluorescence), electrochemical characterization (Cyclic voltammetry) are similar as mentioned in our previous papers.[1-4] The time of flight (TOF)[1] and electrolumuinscence[3] instrumental and device fabrication details are similar as described in our previous paper. The final materials, **3a-d** were synthesized using Microwave synthesis reactor Monowave 300 from Anton paar.

2. Synthesis and Characterization details:

2.1 Synthesis of precursor 2. The precursor **2** was prepared by following earlier methods.[5] Briefly, perylene-3,4,9,10-tetracarboxylic dianhydride (170 mg, 1 equiv.) was taken in a 250 ml round bottom flask. 170 ml of 0.1 M KOH solution is added and heated at 70 °C for about 2 hours. The clear green fluorescent solution of reaction mixture appears due to the formation of tetra potassium carboxylate anion. The solution was allowed to cool down to room temperature, filtered and acidified with dilute hydrochloric acid to get a solution with pH value of 8-9. To this solution, was then added propargyl bromide (412 mg, 8 equiv.) and tetraoctyl ammonium bromide (TOAB, 190 mg, 0.8 equiv.). The reaction mixture was refluxed under vigorous stirring for overnight. The solution became almost colourless and red or brown coloured insoluble material floats on the surface. The crude reaction mixture was extracted using chloroform. The reaction mixture was purified through column chromatography by using 1:1 hexane/ethyl acetate (EtOAc) as eluent. After column chromatography the obtained compound was washed several times with methanol and hexane to get pure product. Yield – 40 %.

^{1}H NMR (400 MHz, $CDCl_3$, δ in ppm): δ 8.23-8.22 (d, 4H, J = 4.00 Hz), δ 8.10-8.08 (d, 4H, J = 8.00 Hz), δ 4.98 (s, 8H), δ 2.59 (s, 4H).

^{13}C NMR (100 MHz, $CDCl_3$, δ in ppm): Due to the limited solubility of compound in the $CDCl_3$ and insolubility in other solvents, we were unable to record the ^{13}C spectra of precursor **2**.

HRMS-ESI (m/z): M^+ 581.1286 (calculated for $C_{36}H_{20}O_8$ = M^+ 581.1236).

2.2 Synthesis of alkyl azides. The alkyl azides were prepared by following earlier methods.[6] Briefly, 0.5 M stock solution of NaN_3 (0.69 g) in DMSO (21 ml) was prepared by stirring the solution for 24 hours at room temperature. After obtaining the clear solution, to 0.5 M solution of NaN_3 (1.1 equiv.), bromoalkane (1 equiv.) was added. After stirring for 24 hours at room temperature, the reaction mixture was extracted with diethyl ether. After evaporation of the solvent, the resulting mixture was evaporated to dryness. Yield of azides ~ 99 %. The formation of the azides was first checked with IR. The appearance of peak at 2096 cm^{-1} in IR corresponds to asymmetric stretching frequency for $C\text{-}N_3$. It also indicates the conversion of bromoalkane to azidoalkane.

2.3 Synthesis of final PTE derivatives, 3a-d

Compound **2** (50 mg, 1 equiv.), corresponding alkyl azide (8 equiv.), $CuSO_4.5H_2O$ (1 equiv.) and sodium ascorbate (0.6 equiv.) were solubilised using the following solvent mixture in a microwave reaction vial (G-10).[7] The solvent mixture is $CHCl_3$ (2 ml)/EtOH (1 ml)/H_2O (1 ml). The reaction mixture was kept at 65 °C for 1 hour with constant stirring under microwave irradiation. The reaction mixture turned out to be brownish-red and the completion of the reaction was determined by the disappearance of the reactant spot on TLC. After that, the crude mixture was extracted with $CHCl_3$/ H_2O. The crude red solid obtained was purified on neutral alumina by using hexane/EtOAc as eluent. Yield: 60 % for **3a**; 63 % for **3b**; 68 % for **3c**; 72 % for **3d**.

Compound **3a**

FT-IR (cm^{-1}): 3427, 3143, 2962, 2930, 2855, 1729, 1591, 1463, 139, 1262, 1158, 1095, 1020, 803, 752, 617.

^{1}H NMR (400 MHz, $CDCl_3$, δ in ppm): δ 8.26-8.24 (d, 4H, J = 8.00 Hz), δ 8.06-8.04 (d, 4H, J = 8.00 Hz), δ 7.80 (s, 4H), δ 5.44 (s, 8H), δ 4.40-4.34 (m, 8H), δ 1.95-1.91 (m, 4H), δ 1.74-1.68 (m, 4H), δ 1.50-1.45 (m, 8H), δ 1.29-1.09 (m, 24H), 0.95-0.93 (d, 12 H), 0.84-0.82 (d, 24H).

^{13}C NMR (100 MHz, $CDCl_3$, δ in ppm): 168.15, 142.37, 131.08, 124.04, 121.63, 114.09, 58.86, 48.74, 39.11, 37.35, 36.88, 31.95, 30.40, 29.72, 29.39, 27.92, 24.53, 22.67, 22.57, 19.27, 14.16.

HRMS-ESI (m/z): M^+ 1313.8132 (calculated for $C_{76}H_{104}N_{12}O_8$ = M^+ 1313.8178).

Compound **3b**

FT-IR (cm^{-1}): 3396, 2925, 2861, 1721, 1587, 1469, 1374, 1275, 1162, 1093, 806, 751, 615.

^{1}H NMR (400 MHz, $CDCl_3$, δ in ppm): δ 8.07-8.05 (d, 4H, J = 8.00 Hz), δ 7.94-7.92 (d, 4H, J = 8.00 Hz), δ 7.83 (s, 4H), δ 5.45 (s, 8H), δ 4.38-4.34 (t, 8H, J = 7.32 Hz), δ 1.92-1.87 (m, 8H), δ 1.34-1.27 (m, 24H), 0.86-0.83 (t, 12H, J = 6.60 Hz).

^{13}C NMR (100 MHz, $CDCl_3$, δ in ppm): 168.13, 142.35, 133.04, 130.98, 129.43, 128.87, 128.56, 124.14, 121.54, 58.83, 50.51, 31.13, 30.25, 26.17, 22.42, 13.96.

HRMS-ESI (m/z): M^+ 1089.5621 (calculated for $C_{60}H_{72}N_{12}O_8$ = M^+ 1089.5674).

Compound **3c**

FT-IR (cm^{-1}): 3392, 2956, 2925, 2850, 1711, 1465, 1277, 1170, 1093, 840, 791, 750, 589.

^{1}H NMR (400 MHz, $CDCl_3$, δ in ppm): δ 8.19-8.17 (d, 4H, J = 8.00 Hz), δ 8.02-8.00 (d, 4H, J = 8.00 Hz), δ 7.80 (s, 4H), δ 5.44 (s, 8H), δ 4.37-4.33 (t, 8H, J = 7.26 Hz), δ 1.92-1.88 (m, 8H), δ 1.41-1.00 (m, 40H), 0.87-0.82 (m, 12H).

^{13}C NMR (100 MHz, $CDCl_3$, δ in ppm): 168.13, 142.35, 133.17, 131.05, 129.51, 128.97, 124.11, 121.60, 58.86, 53.46, 50.51, 31.86, 30.29, 29.48, 29.40, 29.27, 29.01, 26.52, 22.67, 14.12.

HRMS-ESI (m/z): M^+ 1201.6976 (calculated for $C_{68}H_{88}N_{12}O_8$ = M^+ 1201.6926).

Compound **3d**

FT-IR (cm^{-1}): 3136, 2958, 2924, 2854, 1724, 1589, 1514, 1466, 1376, 1271, 1158, 1052, 974, 845, 747, 581, 611.

^{1}H NMR (400 MHz, $CDCl_3$, δ in ppm): δ 8.22-8.20 (d, 4H, J = 8.00 Hz), δ 8.04-8.02 (d, 4H, J = 8.00 Hz), δ 7.80 (s, 4H), δ 5.44 (s, 8H), δ 4.36-4.33 (t, 8H, J = 7.26 Hz), δ 1.90-1.88 (m, 8H), δ 1.31-1.22 (m, 56H), 0.86-0.83 (t, 12H, J = 6.70 Hz) .

^{13}C NMR (100 MHz, $CDCl_3$, δ in ppm): 168.13, 142.35, 133.17, 131.05, 129.51, 128.97, 124.11, 121.60, 58.86, 53.46, 50.51, 31.86, 30.29, 29.48, 29.40, 29.27, 29.01, 26.52, 22.67, 14.12.

HRMS-ESI (m/z): M$^+$ 1313.8115 (calculated for $C_{76}H_{104}N_{12}O_8$ = M$^+$ 1313.8178).

3. NMR Spectral data:

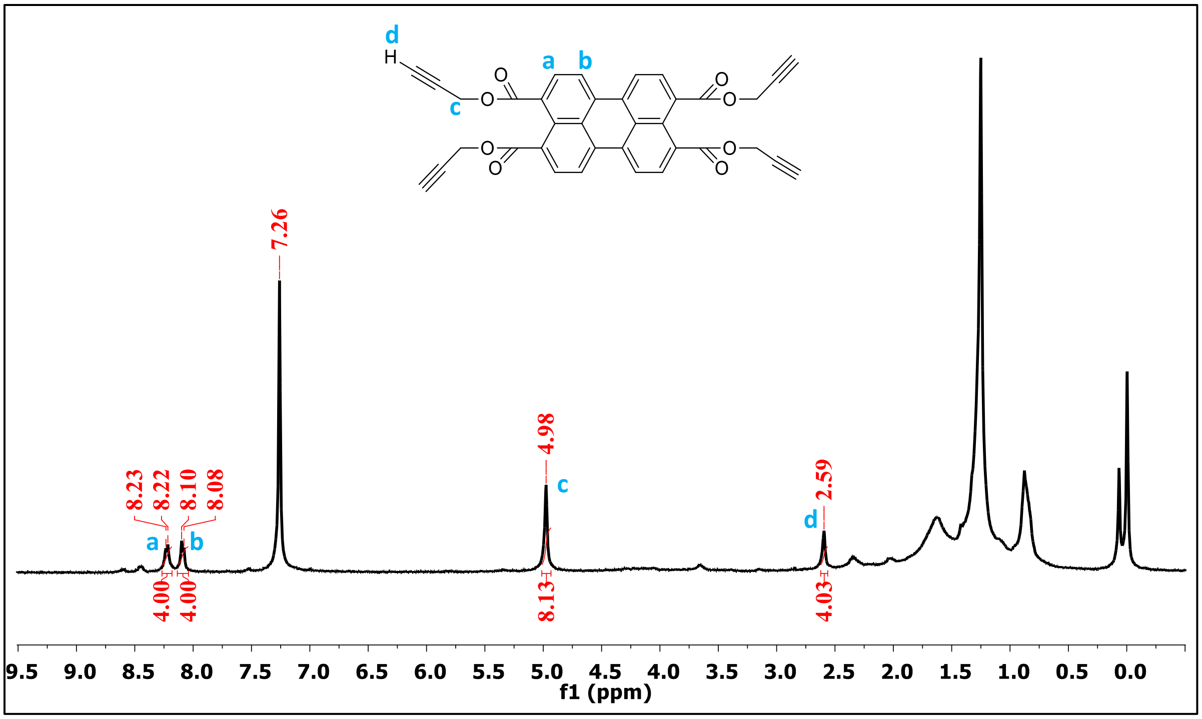

Figure S1. ^{1}H NMR spectrum of precursor **2**.

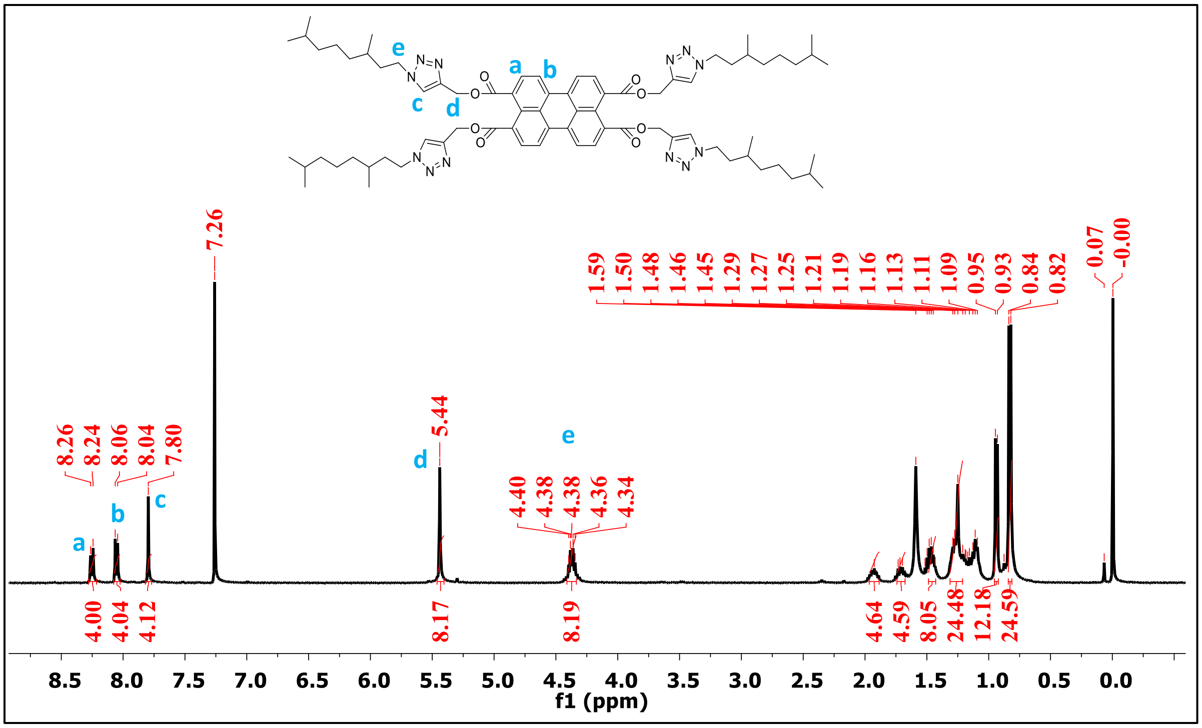

Figure S2. ^{1}H NMR spectrum of **3a**.

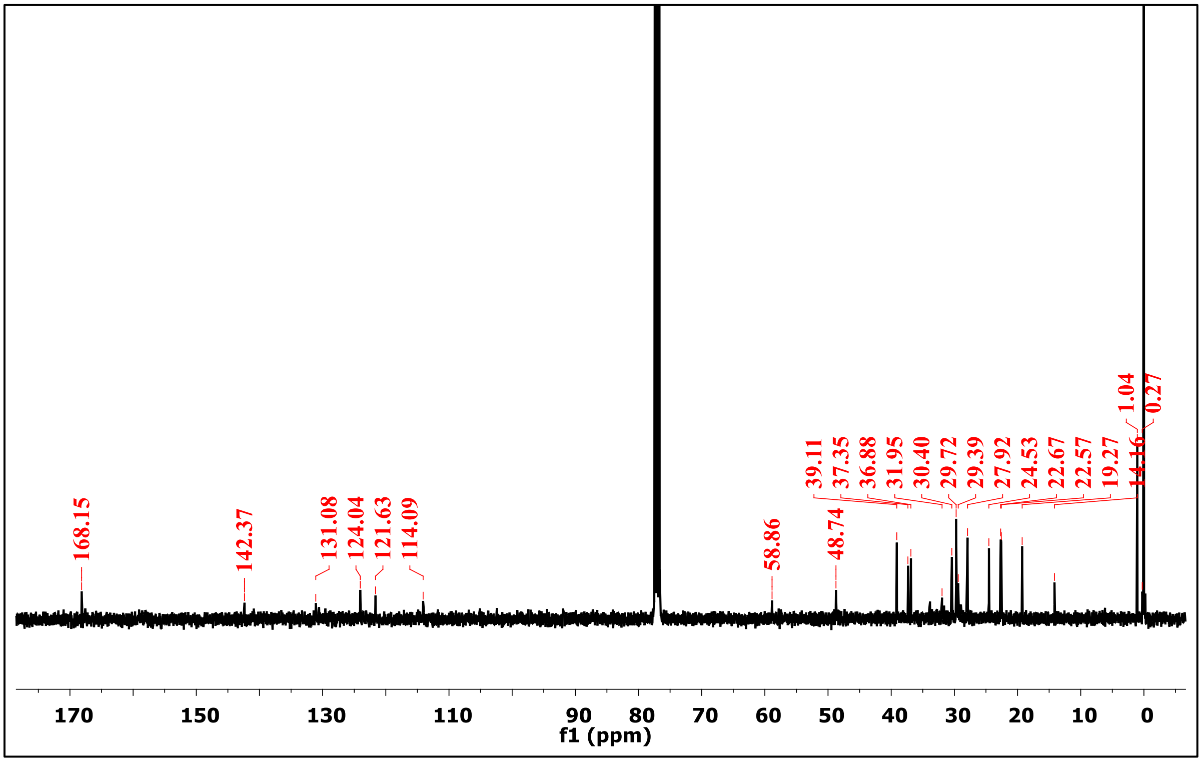

Figure S3. ^{13}C NMR spectrum of **3a**.

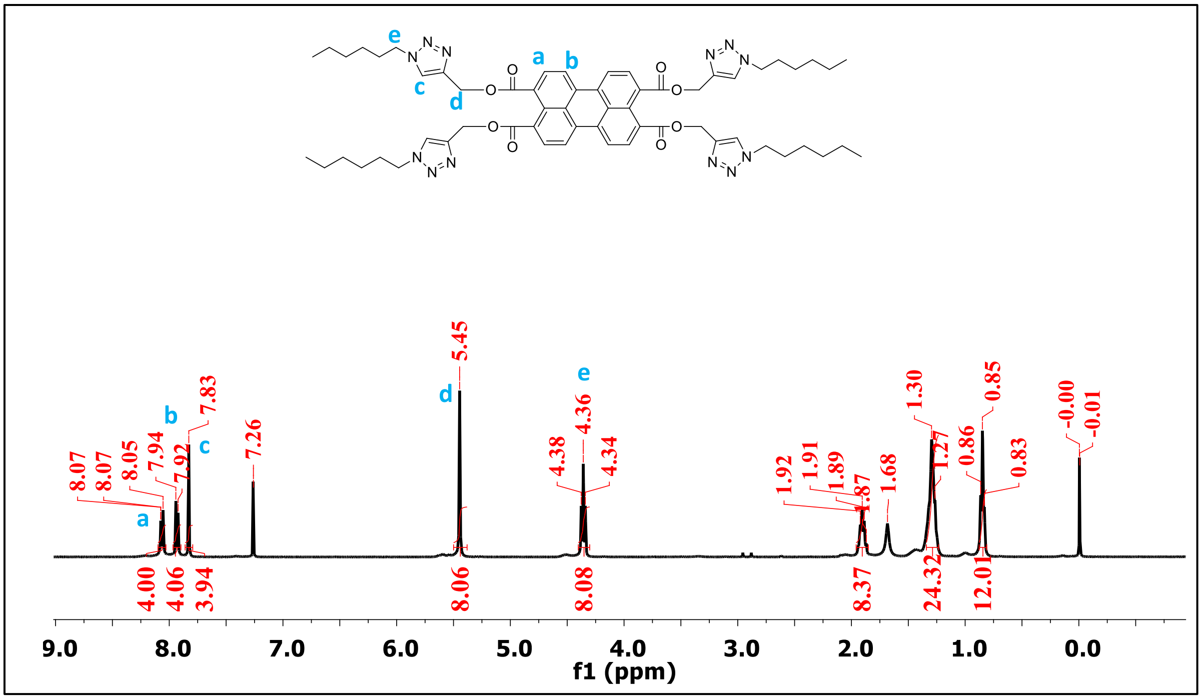

Figure S4. ^{1}H NMR spectrum of **3b**.

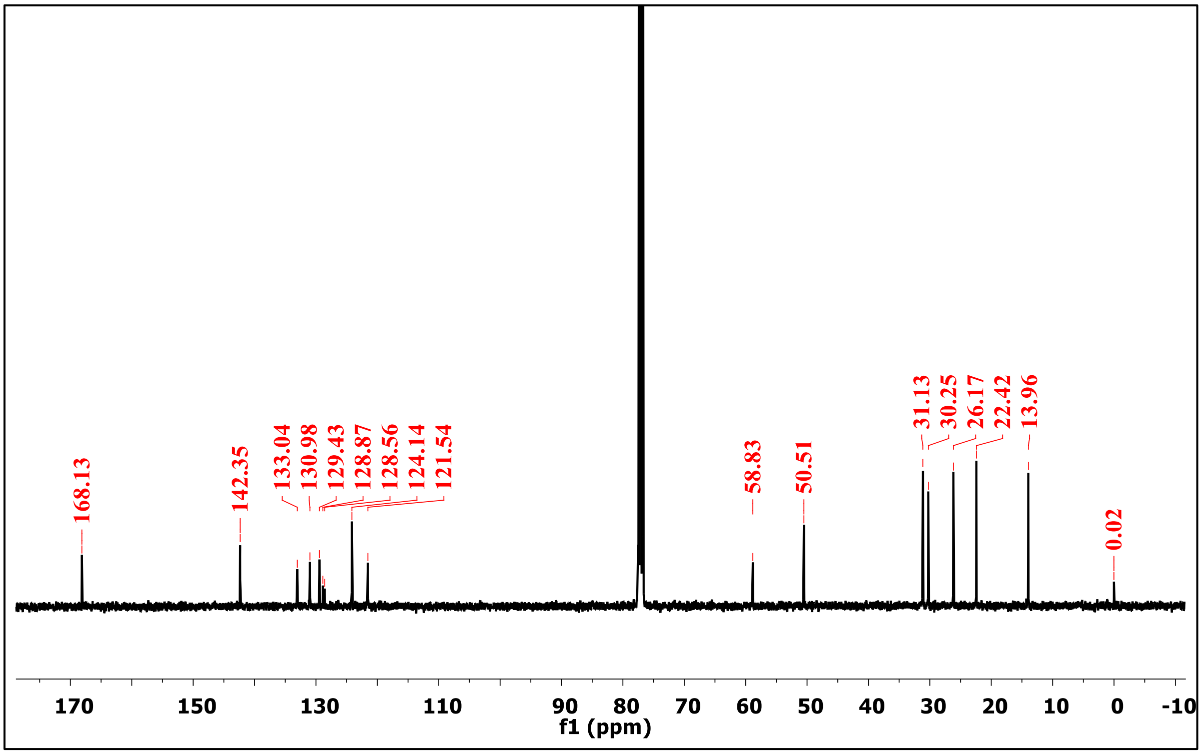

Figure S5. ^{13}C NMR spectrum of **3b**.

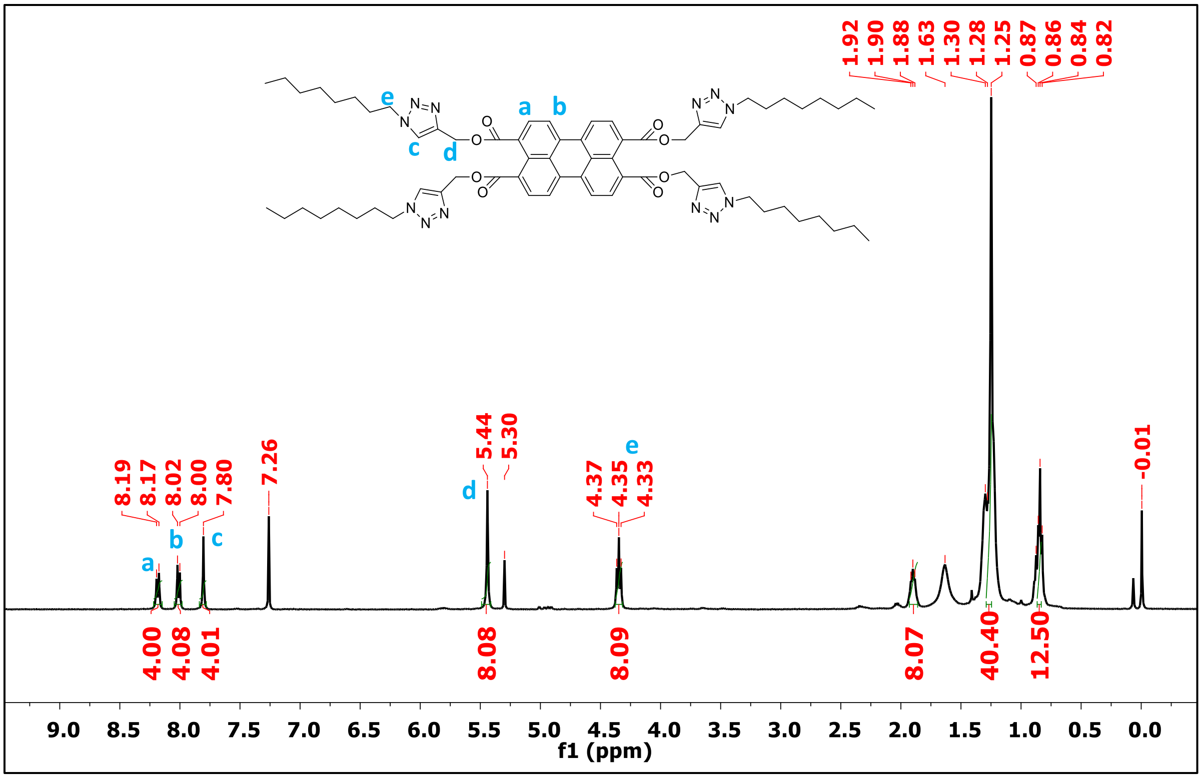

Figure S6. ^{1}H NMR spectrum of **3c**.

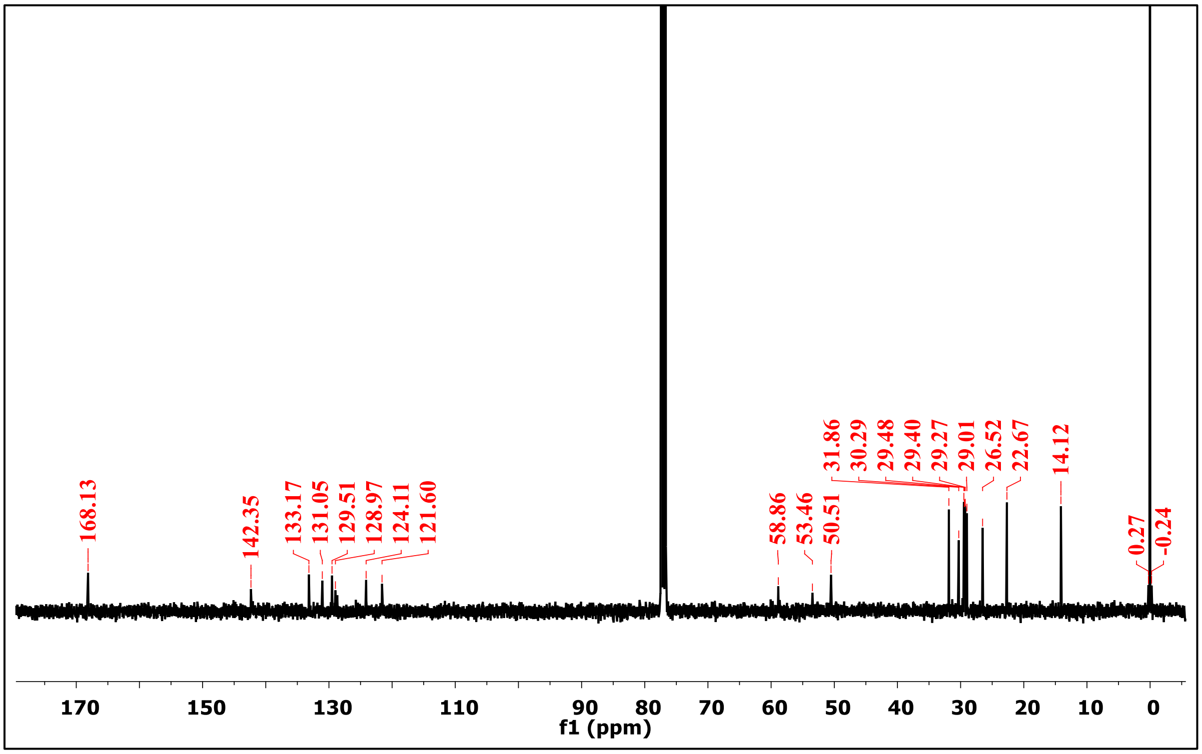

Figure S7. ^{13}C NMR spectrum of **3c**.

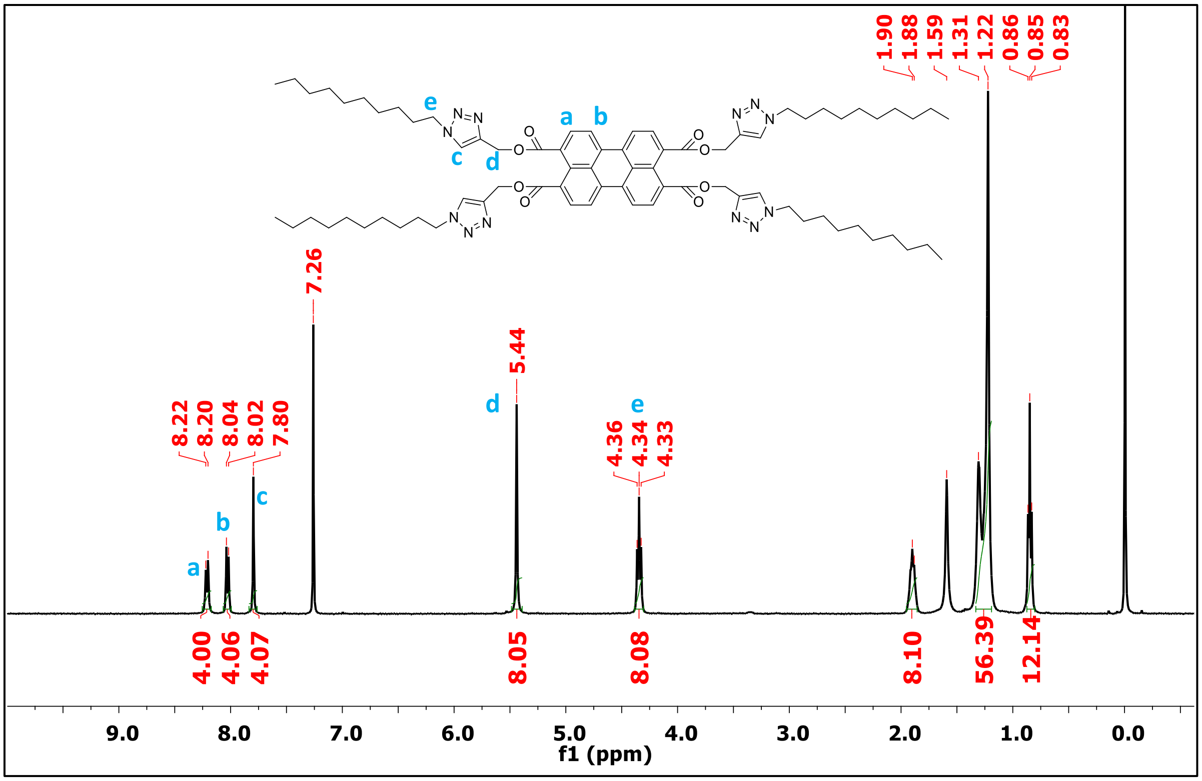

Figure S8. ^{1}H NMR spectrum of **3d**.

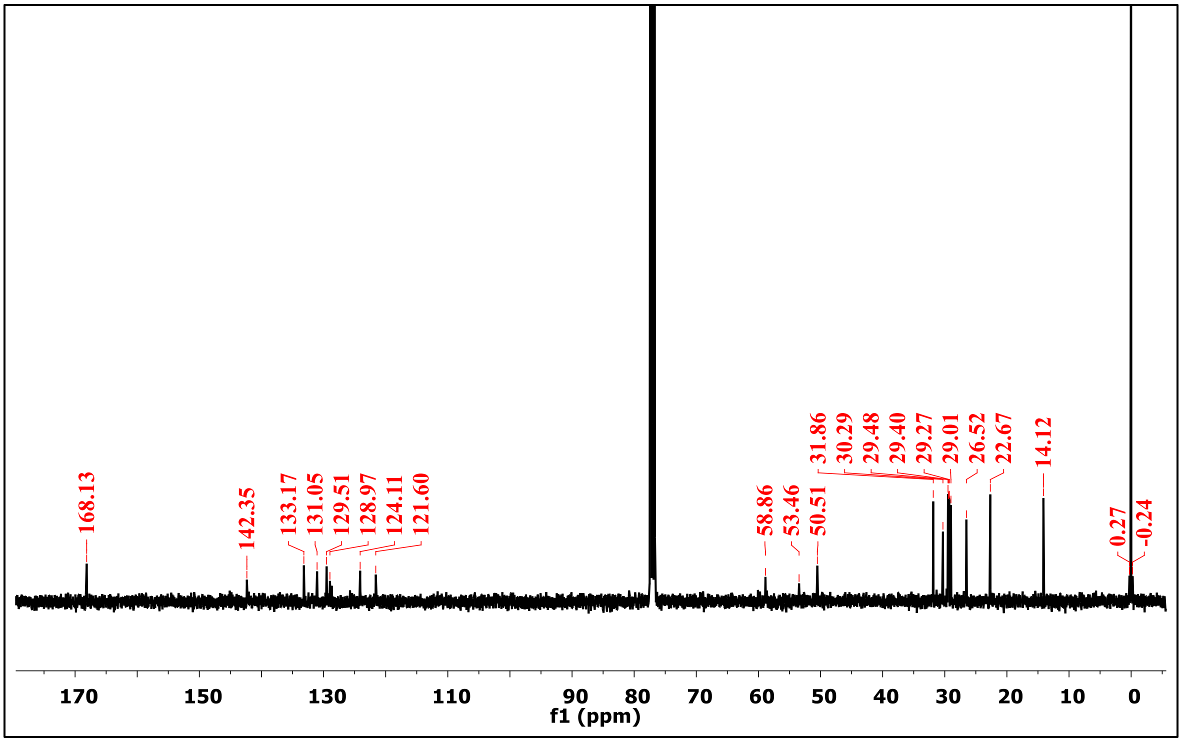

Figure S9. ^{13}C NMR spectrum of **3d**.

4. HRMS spectral data:

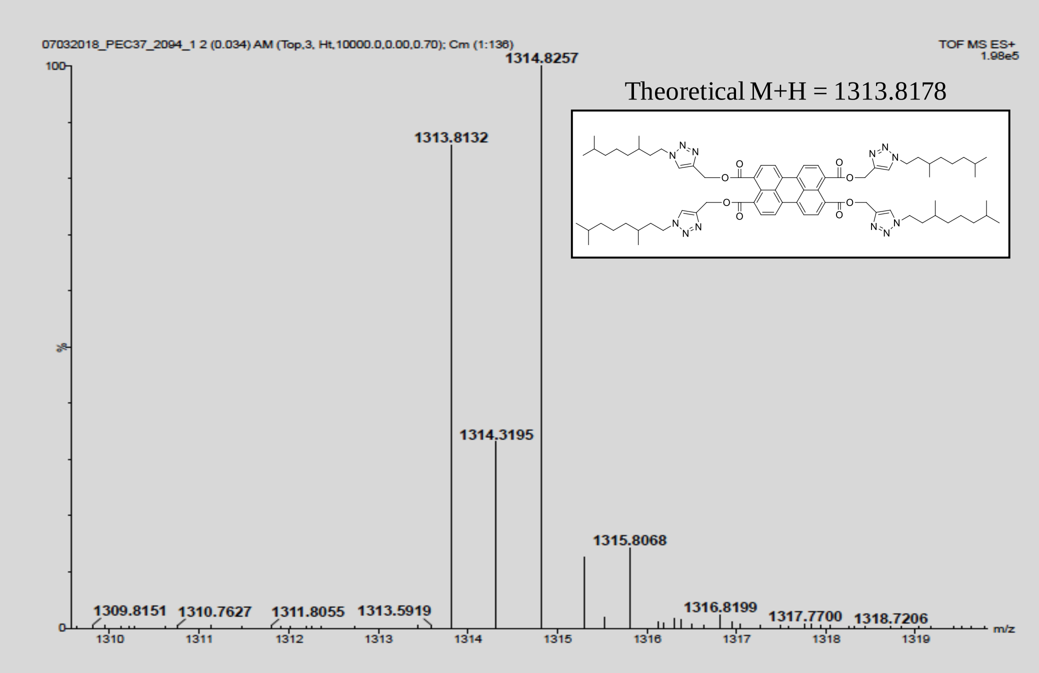

Figure S10. HRMS spectrum of **3a**.

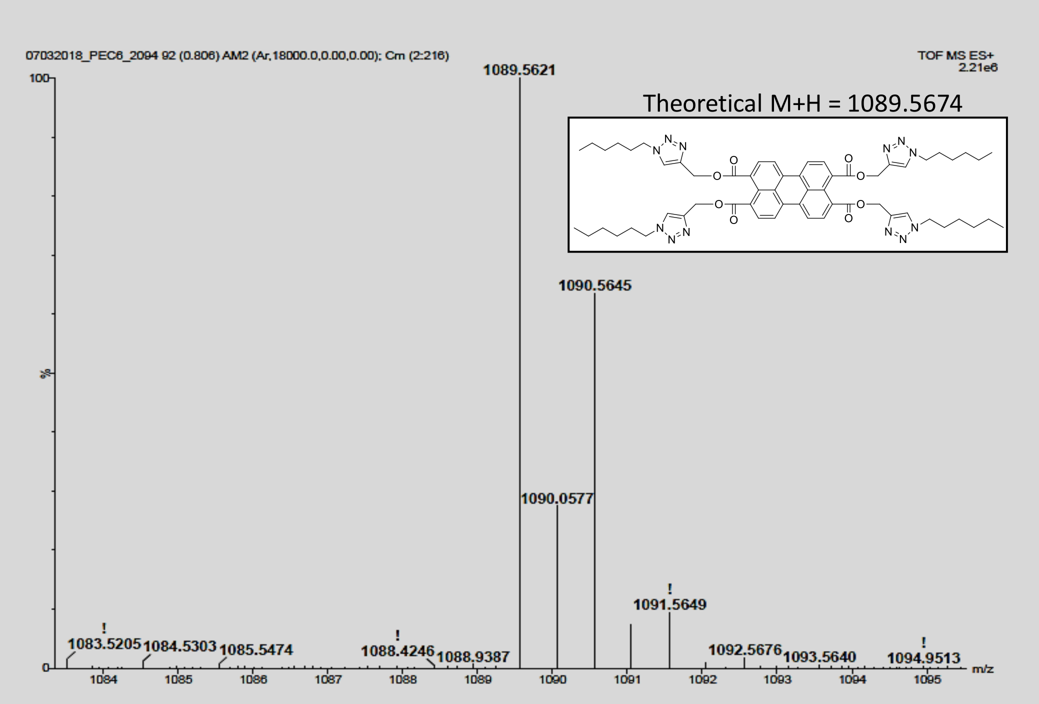

Figure S11. HRMS spectrum of **3b**.

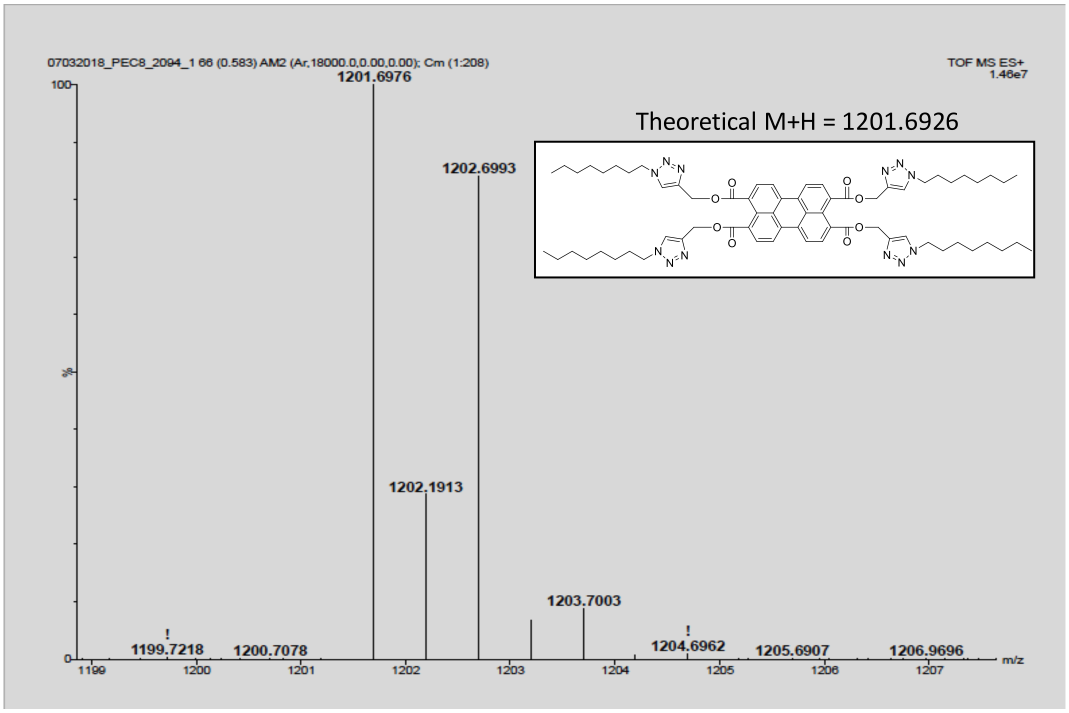

Theoretical M+H = 1201.6926

Figure S12. HRMS spectrum of 3c.

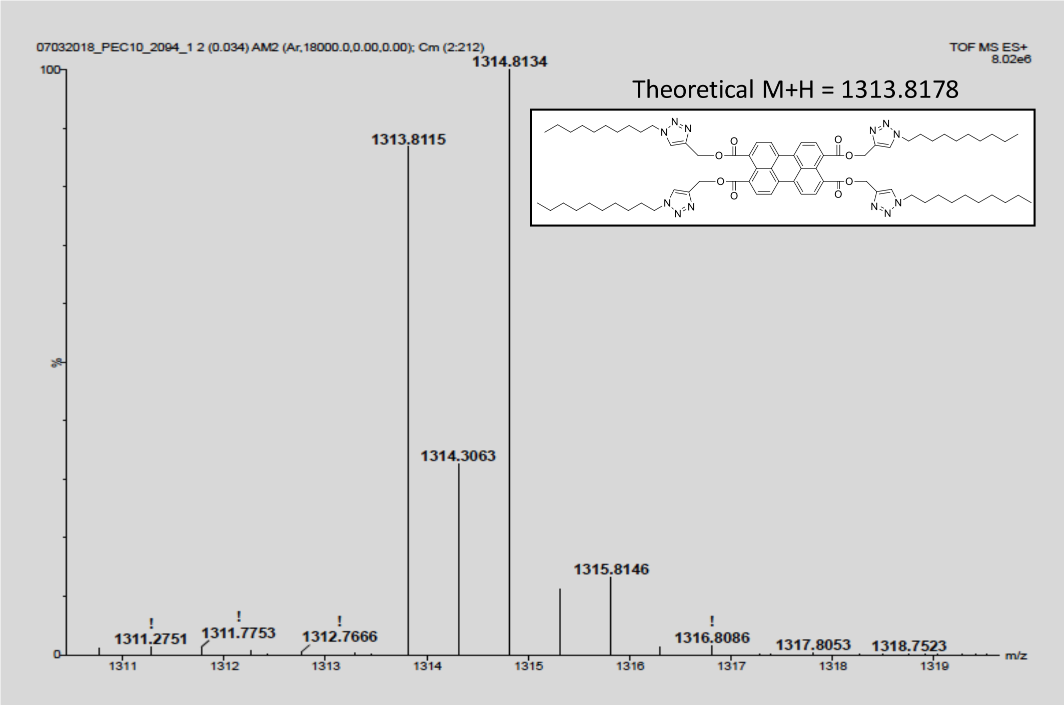

Theoretical M+H = 1313.8178

Figure S13. HRMS spectrum of **3d**.

5. Thermogravimetric analysis (TGA) data:

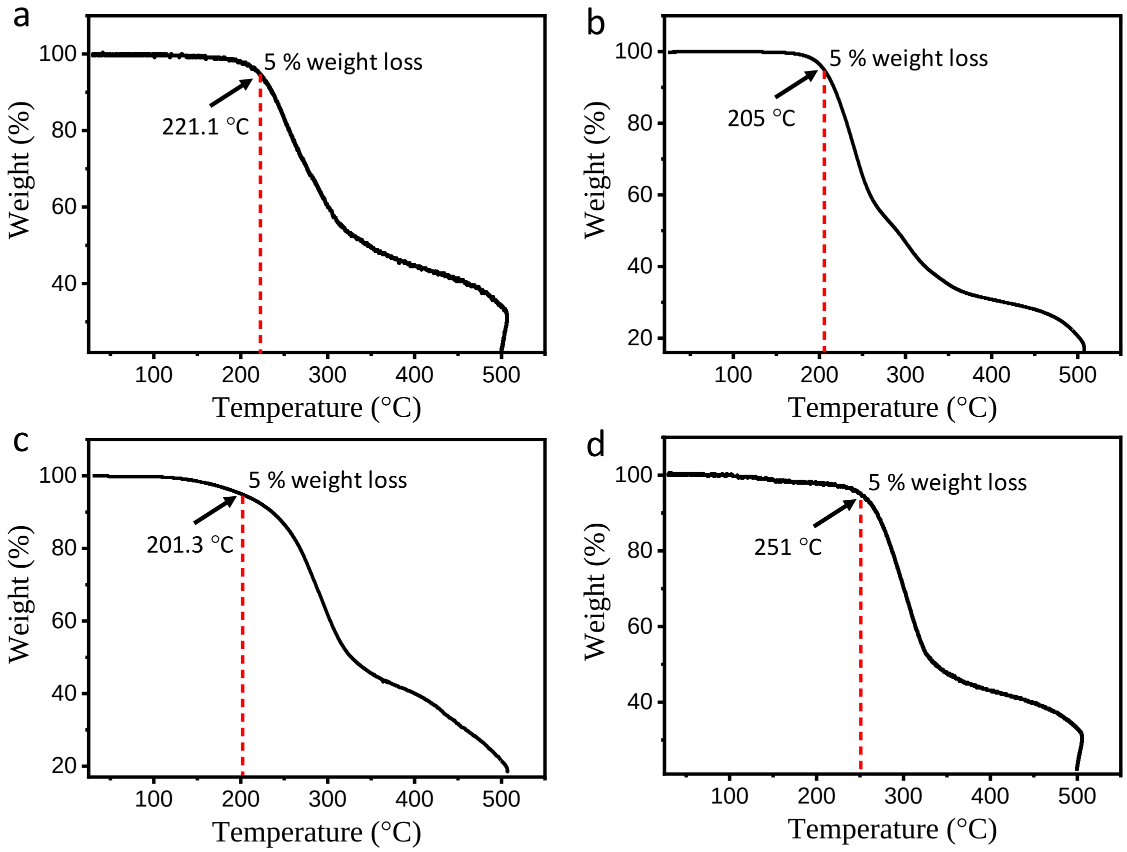

Figure S14. TGA curves of PTE derivatives: (a) **3a** showing stability till 221.1 ˚C; (b) **3b** showing stability till 205 ˚C; (c) **3c** showing stability till 201.3 ˚C; (d) **3d** showing stability up to 251 ˚C. **Note**: The shown temperature is when the compounds undergo 5% weight loss.

6. Polarized optical microscopic (POM) images:

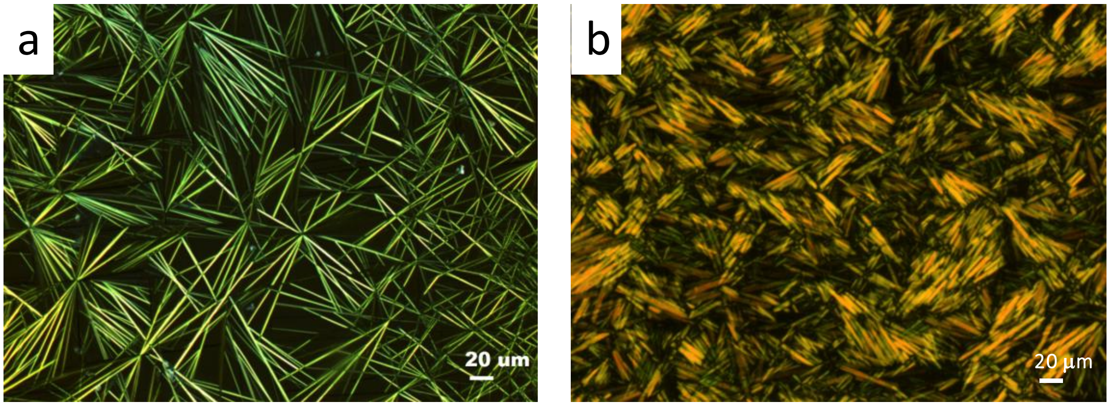

Figure S15. Polarized microscopic images of compound **3a** (a) at 88.1 °C (as also shown in main manuscript in Figure 1a) and (b) obtained on shearing the textures at 88.1 °C.

7. Differential scanning calorimetry (DSC) thermogram:

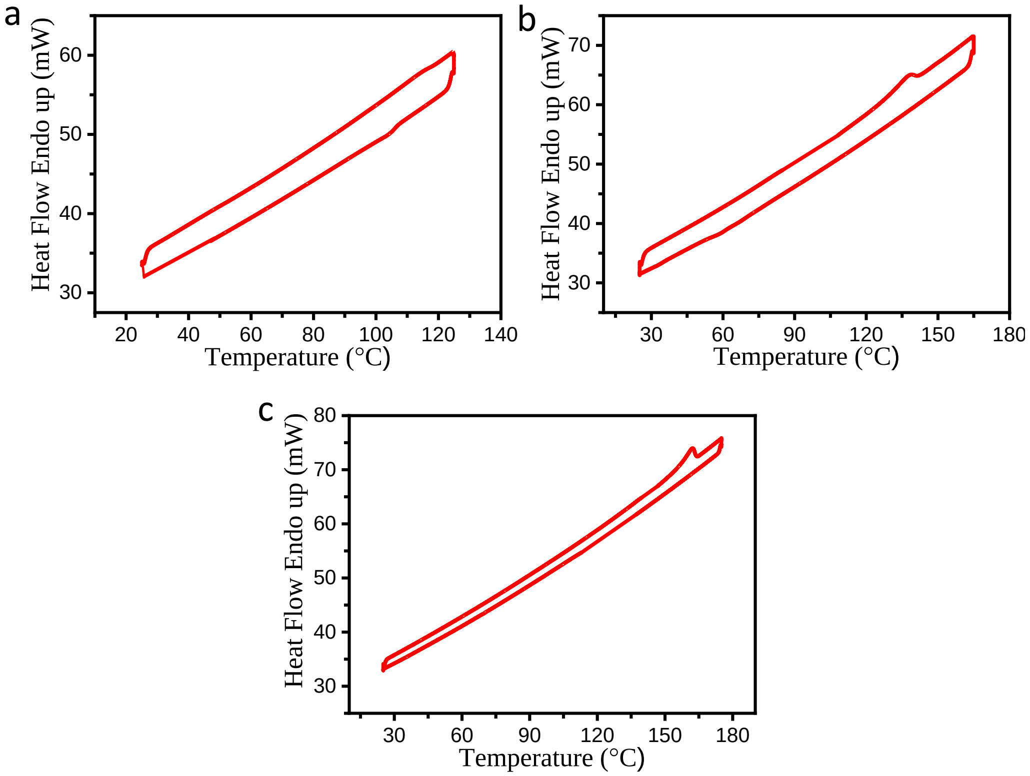

Figure S16. DSC thermogram of PTE derivatives: (a) **3a**; (b) **3c**; (d) **3d**, recorded with the scan rate of 10 °C/min.

Table S1. Thermal behavior of PTE derivatives. [a]

Compound	Phase transition temperatures (°C)
3a	Col$_{ro}$ 115.5^{b} (0.51) Iso Iso 104.2^{b} (1.24) Col$_{ro}^{d}$
3b	Col$_{ro}$ 175^{c} Iso Iso 169^{c} Col$_{ro}^{d}$
3d	Col$_{ro}$ 162.2^{b} (23.92) Iso Iso 151^{c} Col$_{ro}^{d}$

[a] Enthalpy values in parentheses in kJ/mol (mentioned also in Table 1 in the main manuscript). [b] Phase transition through DSC. [c] Phase transition through POM. [d] Columnar rectangular structure (Col$_{ro}$): columnar rectangular morphology at lower temperatures (Col$_{ro1}$) is different from that at higher temperatures (Col$_{ro2}$) as observed from temperature-dependent XRD studies on cooling from the isotropic, however in DSC thermograms, no such transition (Col$_{ro1}$ to Col$_{ro2}$) observed, might be due to small structural changes within the same lattice.

8. (a) X-ray diffraction study:

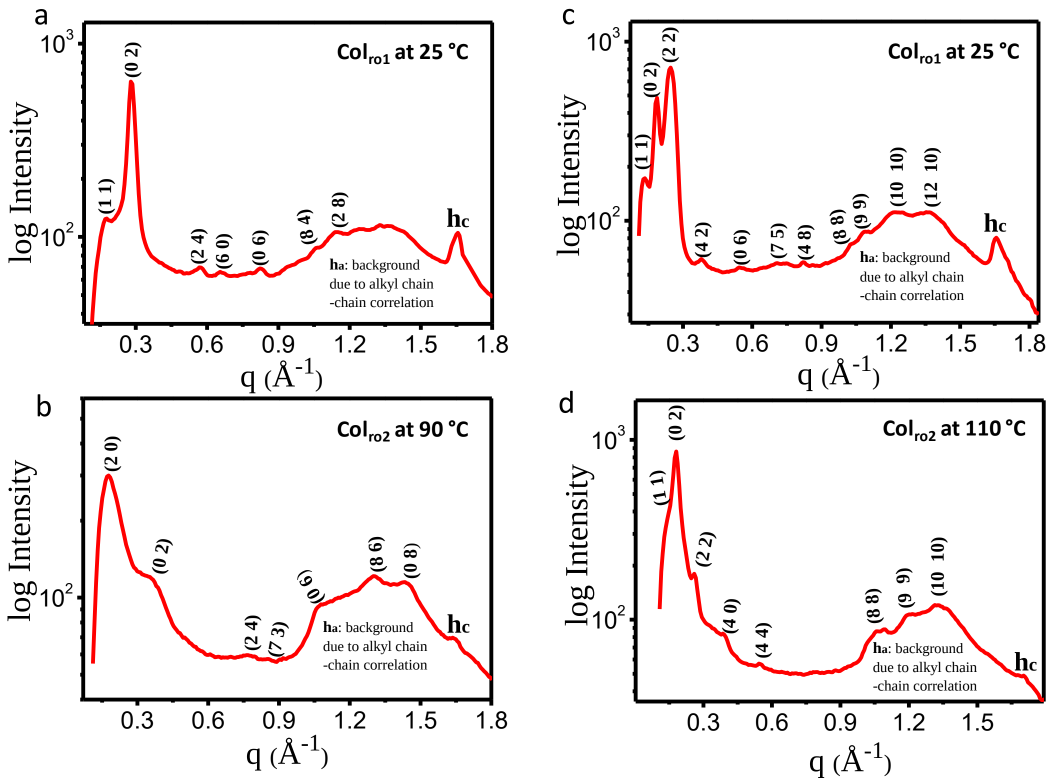

Figure S17. XRD pattern of **3b**: (a) Col$_{ro1}$ phase at 25 °C and (b) Col$_{ro2}$ phase at 90 °C obtained on cooling the isotropic melt (cooling rate 10 °C/min). XRD pattern of **3d**: (c) Col$_{ro1}$ phase at 25 °C and (d) Col$_{ro2}$ phase at 110 °C obtained on cooling the isotropic melt (cooling rate 10 °C/min).

(b) Systematic temperature dependent XRD study:

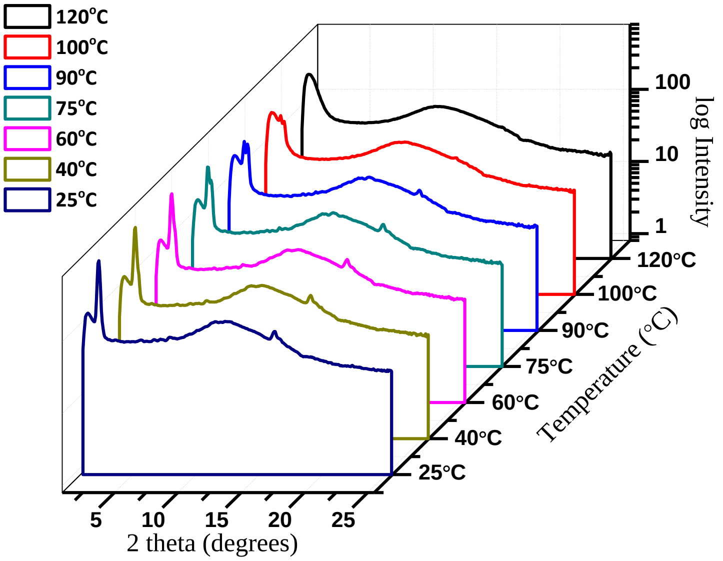

Figure S18. Temperature-dependent XRD studies for **3a** from room temperature to their respective isotropic temperatures on cooling from the isotropic phase.

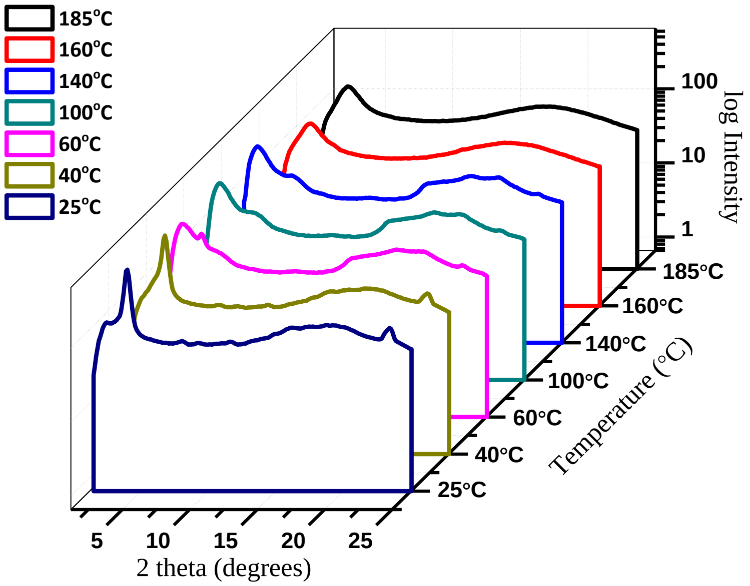

Figure S19. Temperature-dependent XRD studies for **3b** from room temperature to their respective isotropic temperatures on cooling from the isotropic phase.

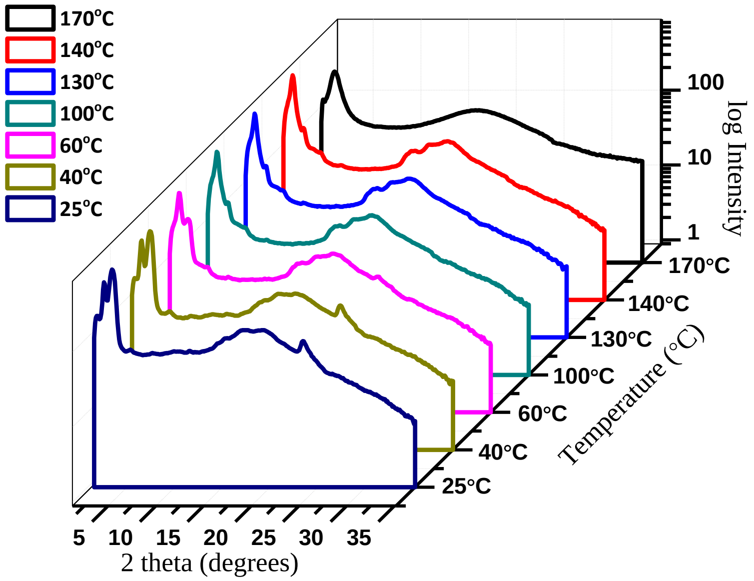

Figure S20. Temperature-dependent XRD studies for **3d** from room temperature to their respective isotropic temperatures on cooling from the isotropic phase.

Table S2. XRD parameters of **3a** in the columnar liquid crystal phase.

Compound	Mesophase	Lattice constants (Å)	$d_{obs}{}^{a}$ (Å)	$d_{cal}{}^{b}$ (Å)	Miller Indices (*hk*)
3a	Col$_{ro1}$ at 25 °C	*a* = 85.36	42.68	42.68	2 0
		b = 53.74	26.87	26.87	0 2
			17.20	17.53	1 3
			11.16	11.37	4 4
			9.40	9.34	9 1
			8.71	8.77	2 6
			7.92	8.06	7 5
			6.67	6.64	2 8
			6.25	6.07	6 8
			5.46	5.68	8 8
			3.87	3.87	$\mathbf{h_c}$
3a	Col$_{ro2}$ at 80 °C	*a* = 83.09	41.56	41.45	2 0
		b = 54.73	27.36	27.37	0 2
			24.71	24.71	3 1
			17.45	17.82	1 3
			15.49	15.24	3 3
			12.20	12.36	6 2
			11.20	11.43	4 4
			9.59	9.73	6 4
			9.04	9.12	0 6
			8.56	8.35	4 6
			7.92	7.78	1 7
			5.51	5.41	7 9
			5.13	5.08	9 9
			3.89	3.89	$\mathbf{h_c}$

[a] d_{obs}: *d*-spacing obtained from XRD experiments; [b] d_{cal}: *d*-spacing calculated by equation: $\frac{1}{d^2} = (\frac{h^2}{a^2} + \frac{k^2}{b^2})$ with $h+k = 2n$, *n* is integer; *h*, *k* are the miller indices belongs to the reflections of centred columnar rectangular (Col$_r$) phases; *a* and *b* are the unit cell parameters, $\mathbf{h_c}$ attributes to *d*-spacing arising from core-core correlation.

Table S3. XRD parameters of **3b** and **3c** in the columnar liquid crystal phase.

Compound	**Mesophase**	**Lattice constants (Å)**	$d_{obs}{}^{a}$ (Å)	$d_{cal}{}^{b}$ (Å)	**Miller Indices (*hk*)**
3b	Col$_{ro1}$ at 25 °C	*a* = 58.50	35.70	35.70	1 1
		b = 45.06	22.53	22.53	0 2
			10.79	10.51	2 4
			9.60	9.75	6 0
			7.57	7.51	0 6
			5.94	6.13	8 4
			5.53	5.53	2 8
			3.80	3.80	$\mathbf{h_c}$
3b	Col$_{ro2}$ at 90 °C	*a* = 70.60	35.30	35.30	2 0
		b = 34.32	17.16	17.16	0 2
			8.10	8.34	2 4
			7.33	7.57	7 3
			5.86	5.72	0 6
			4.83	4.80	8 6
			4.38	4.29	0 8
			3.80	3.80	$\mathbf{h_c}$
3c	Col$_{ro}$ at 60 °C	*a* = 54.70	44.59	44.60	1 1
		b = 77.04	38.52	38.52	0 2
			22.26	22.30	2 2
			19.35	19.26	0 4
			14.56	14.83	1 5
			5.94	6.04	8 6
			5.34	5.32	9 7
			4.97	4.76	10 8
			3.90	3.90	$\mathbf{h_c}$

[a] d_{obs}: experimental *d*-spacing; [b] d_{cal}: calculated *d*-spacing by using the relation: $\frac{1}{d^2} = (\frac{h^2}{a^2} + \frac{k^2}{b^2})$ with $h+k = 2n$, *n* is integer; *h*, *k* are the miller indices of the reflections corresponding to the centred columnar rectangular (Col$_r$) phases; *a* and *b* are the unit cell parameters, $\mathbf{h_c}$ spacing appear due to core-core correlation.

Table S4. XRD parameters of **3d** in the columnar liquid crystal phase.

Compound	**Mesophase**	**Lattice constants (Å)**	d_{obs}^{a} (Å)	d_{cal}^{b} (Å)	**Miller Indices (*hk*)**
3d	Col$_{ro1}$ at 25 °C	*a* = 78.10	50.83	50.84	1 1
		b = 66.98	33.49	33.49	0 2
			25.45	25.42	2 2
			16.73	16.87	4 2
			11.39	11.16	0 6
			8.71	8.57	7 5
			7.66	7.69	4 8
			6.14	6.36	8 8
			5.80	5.65	9 9
			5.17	5.08	10 10
			4.60	4.67	12 10
			3.80	3.80	**h$_c$**
3d	Col$_{ro2}$ at 110 °C	*a* = 56.80	47.14	47.14	1 1
		b = 45.08	34.69	34.70	0 2
			23.57	23.57	2 2
			16.05	16.06	4 0
			11.57	11.78	4 4
			5.84	5.89	8 8
			5.23	5.24	9 9
			4.71	4.71	10 10
			3.68	3.68	**h$_c$**

$^{a}d_{obs}$: experimental *d*-spacing; $^{b}d_{cal}$: calculated *d*-spacing by using the relation: $\frac{1}{d^2} = (\frac{h^2}{a^2} + \frac{k^2}{b^2})$ with $h+k = 2n$, *n* is integer; *h*, *k* are the miller indices of the reflections corresponding to the centred columnar rectangular (Col$_r$) phases; *a* and *b* are the unit cell parameters, **h$_c$** spacing appear due to core-core correlation.

9. Photophysical study:

a. Thin-film state Absorption and Emission studies

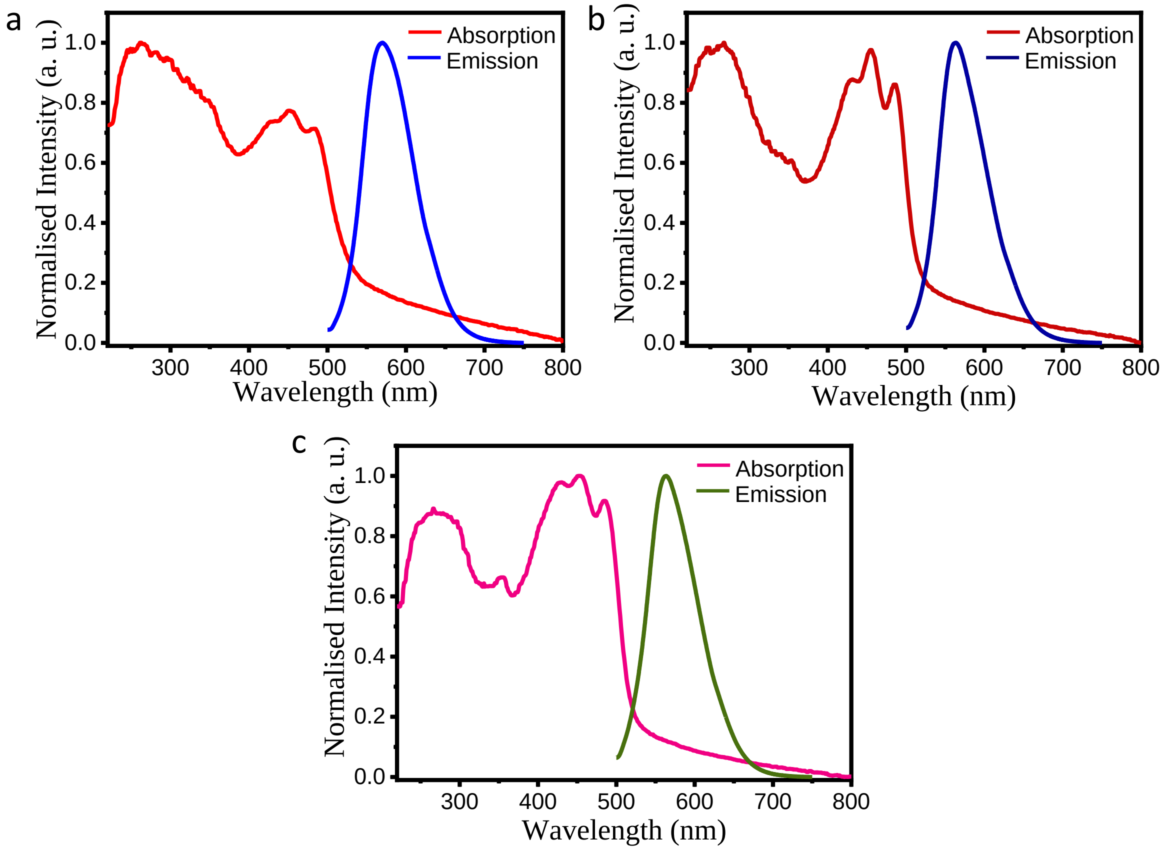

Figure S21. Absorption and emission spectra of perylene derivatives in thin-film (prepared by drop-casting the millimolar solution of the respective compounds in DCM): (a) **3b**; (b) **3c**; (c) **3d**.

b. Quantum yield measurements

The quantum yield calculations were performed by using the procedure reported in our previous paper.[4]

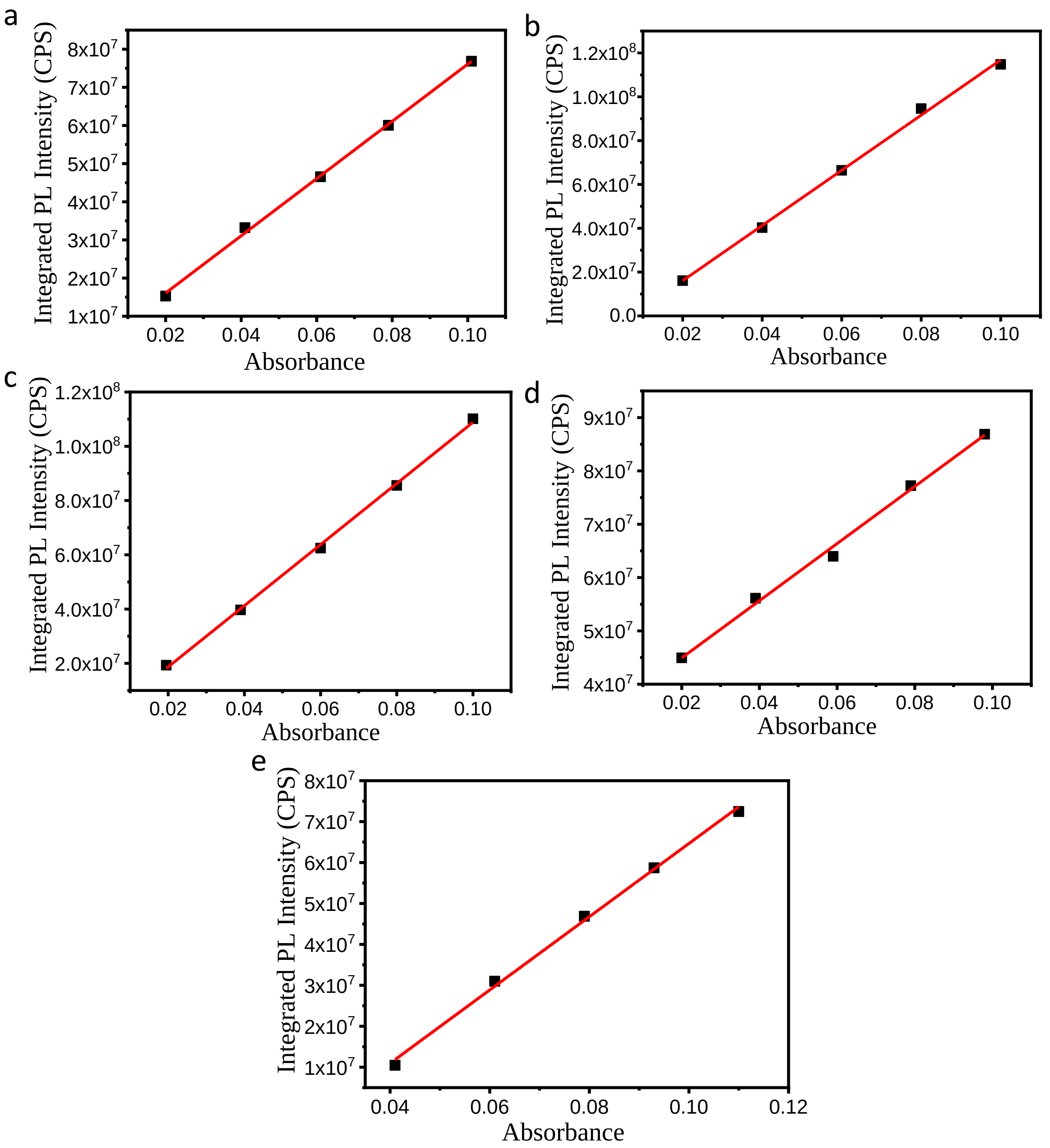

Figure S22. Plots of integrated photoluminescence intensity vs absorbance: (a) **3a**; (b) **3b**; (c) **3c**; (d) **3d**, (λ_{exc}= 446 nm); (e) 0.1 M fluorescein in aq. NaOH solution (λ_{exc}= 491 nm).

10. Cyclic Voltammetry:

For CV measurements, millimolar solutions of the compounds in dichloromethane and 0.1 M tetrabutylammonium hexafluorophosphate solution as a supporting electrolyte were used to perform the CV studies with scan rate of 50 mV/s. For the determination of highest occupied molecular orbitals (HOMO) and lowest occupied molecular orbitals (LUMO) levels, the first oxidation potentials and reduction potential peak onsets were taken into account.

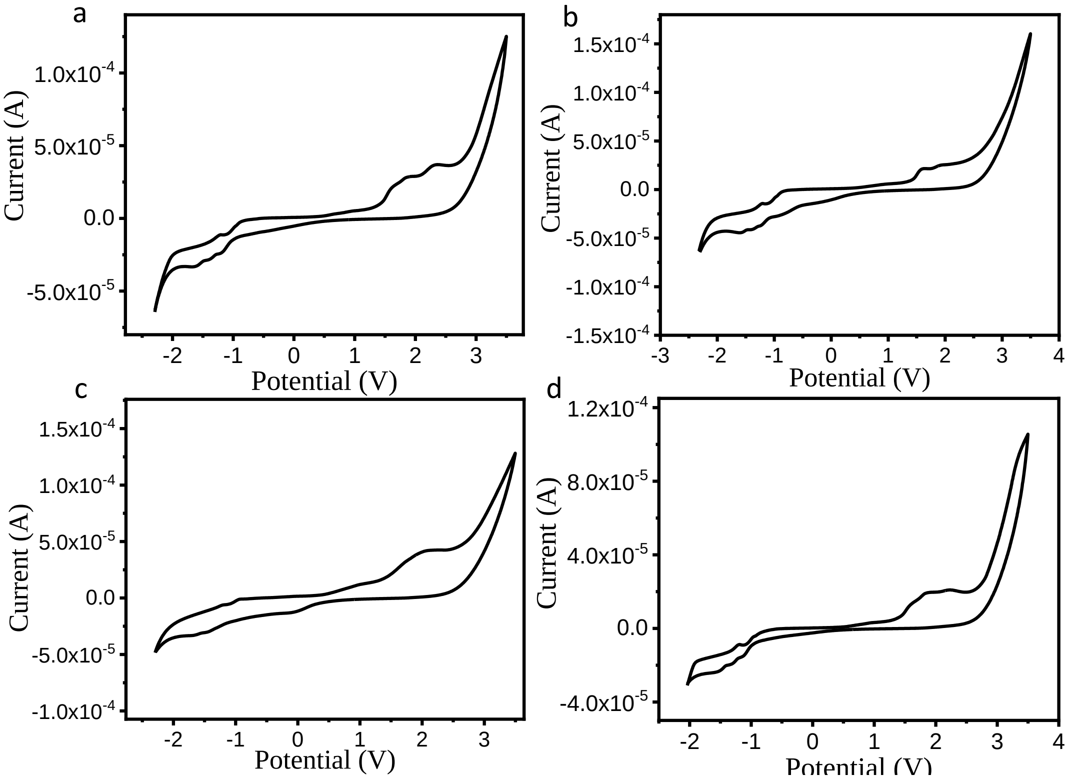

Figure S23. Cyclic Voltammogram for compound (a) **3a** (provided also in the main manuscript as Fig. 3c); (b) **3b**; (c) **3c**; (d) **3d** in HPLC DCM solution of tetrabutylammonium hexafluorophosphate (0.1 M) at scanning rate of 50 mV/s.

11. Ultraviolet photoelectron spectroscopy (UPS):

For UPS measurement, a 2 mg/ml solution of compounds (**3a-d**) in anhydrous chloroform was stirred at 60 °C for 1h. The solution was subsequently spin coated on cleaned indium tin oxide (ITO) substrates at 2000 rpm for 60 s. The HOMO levels are derived from the formula: $E_{HOMO,UPS} = 21.2-(E_{cut\text{-}off}-E_{Fermi})$ where $E_{cut\text{-}off}$ and E_{Fermi} are the kinetic energy obtained at the cut-off (higher energy side) and Fermi edge (lower energy side) of the UPS spectra.

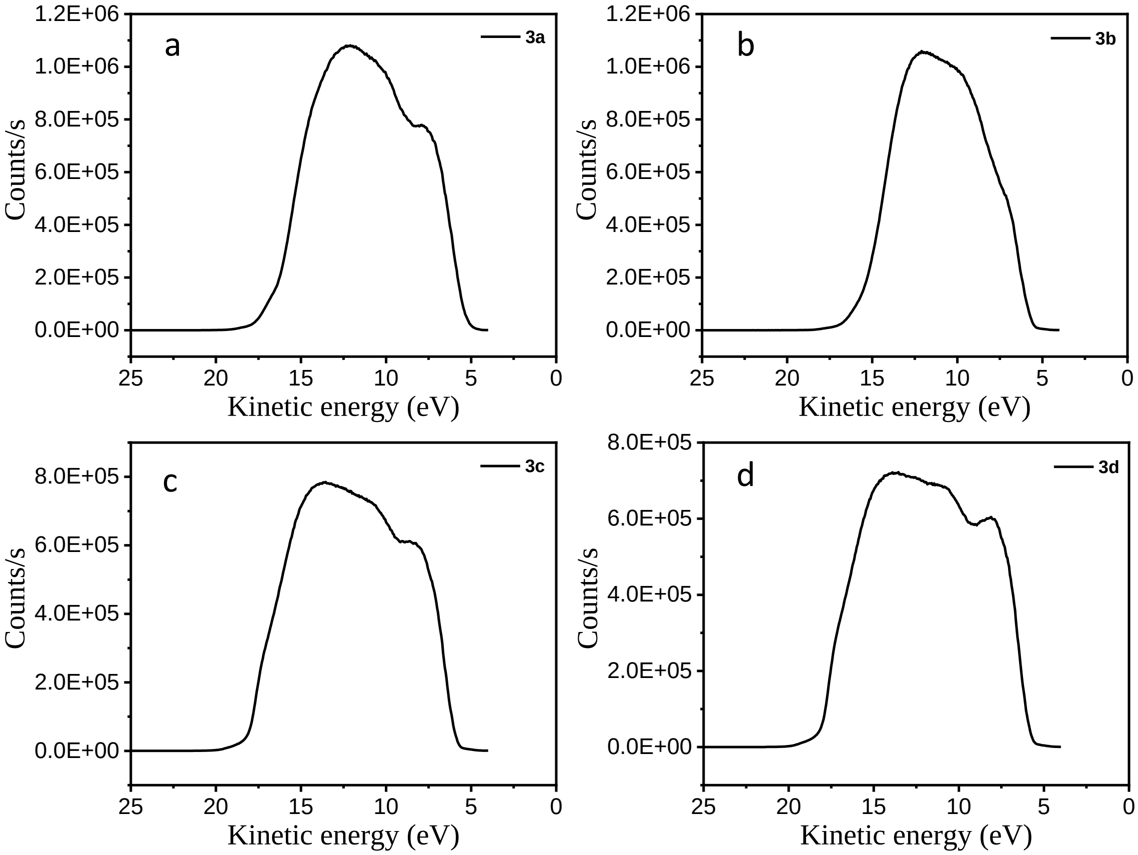

Figure S24. UPS spectra obtained in spin-coated thin-film of compound (a) **3a**; (b) **3b**; (c) **3c**; (d) **3d** on ITO substrates.

12. DFT study:

The geometrical optimization of the molecules **3a-d** was carried out by DFT calculations using B3LYP functional with 6-31G(d,p) basis set.

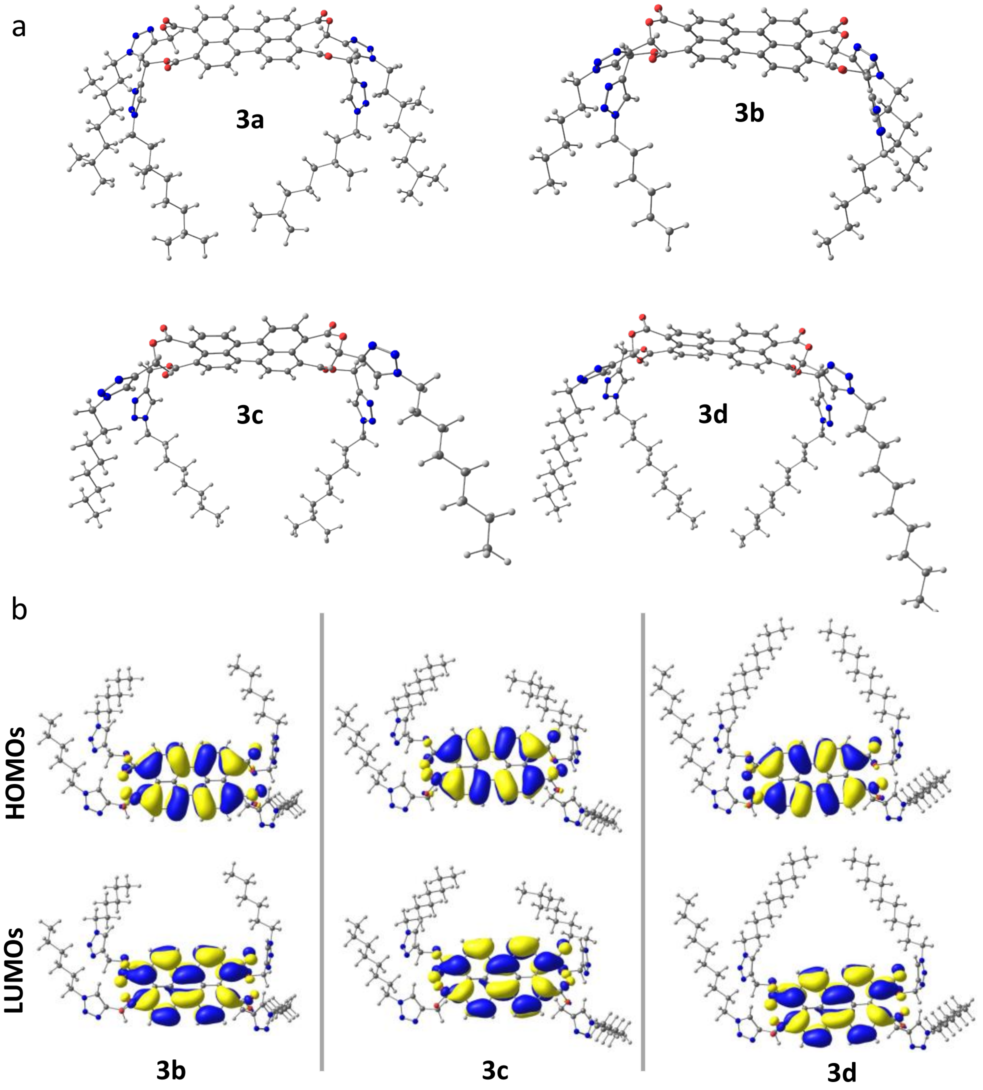

Figure S25. (a) Energy minimized structures and (b) Molecular orbital calculations by DFT method at the B3LYP/6-31G (d,p) level.

13. Electroluminescent (EL) behavior of the 3a derivative:

EL study by varying different hosts:

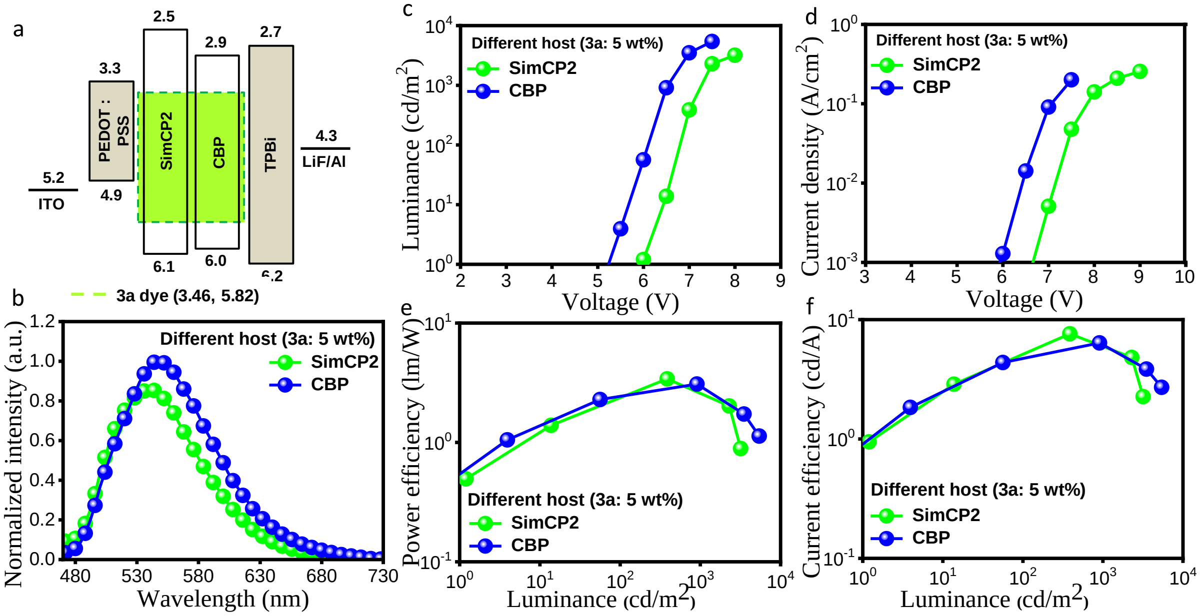

Figure S26. (a) Energy level schematic diagram; (b) electroluminescent spectra (EL); (c) Luminance-voltage; (d) current density-voltage; (e) power efficiency-luminance and (f) current efficiency-luminance plots of the solution-processed OLED device with 5 wt% of **3a** emitter in SimCP2 and CBP host.

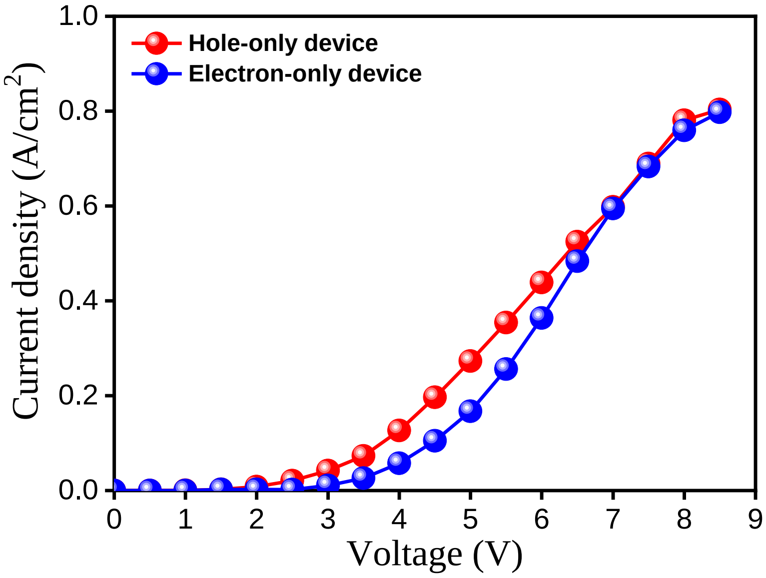

Figure S27. Current density versus Voltage plot of hole-only devices (HOD) and electron-only devices (EOD) of the emitter material **3a** with device configuration-HOD: ITO/PEDOT:PSS/**3a**/LiF/Al and EOD: ITO/**3a**/TPBi/LiF/Al, respectively.

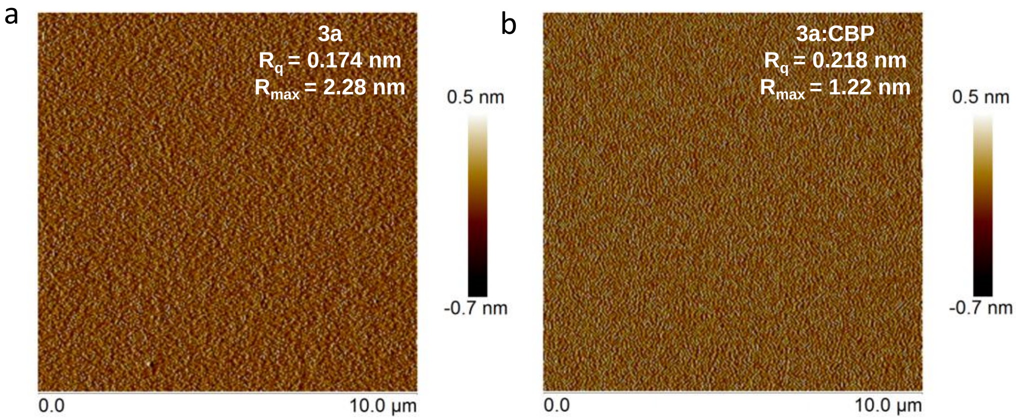

Figure S28. AFM images of (a) **3a** and (b) **3a**:CBP (5 wt% **3a** dopant concentration) spin-coated and cured on ITO glass recorded in tapping mode.

14. TD-DFT and NTO calculations:

Excited states were calculated by time-dependent DFT (TD-DFT) calculations within the Tamm–Dancoff approximation (TDA)[8-10] using the ground state optimized geometries.

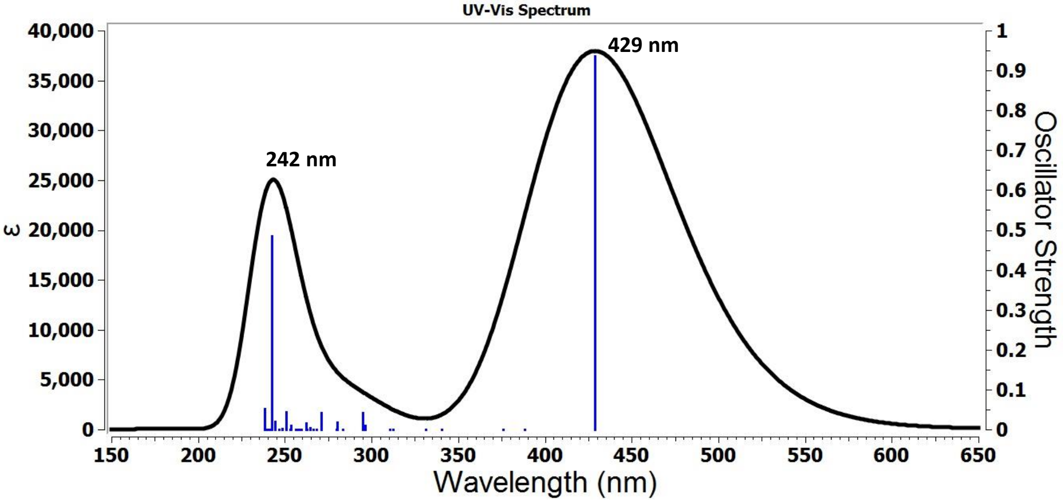

Figure S29. TD-DFT simulated UV-vis absorption spectra of compound **3a** (no. of states considered = 40).

The singlet energy (E_S) of material **3a** calculated from the fluorescence spectra (at room temperature) is found to be 2.52 eV (calculated from emission maxima (recorded in THF)) while E_S = 2.89 eV has been estimated from TD-DFT calculation.

No phosphorescent spectra of **3a** is observed (as performed in THF at 77 K) which is indicative of low density of the T_1 state in **3a**. The similar fact has been reported in the literature.[11] While from TD-DFT the calculated triplet energy of the T_1 state is E_T = 1.79 eV.

Table S5. Calculated natural transition orbitals (NTO) of singlet and triplet excited states.

Excited states (Energies)	**Hole**	**Particle**	**Excited states (Energies)**	**Hole**	**Particle**
S_1 **(2.89 eV)**	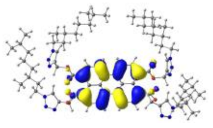	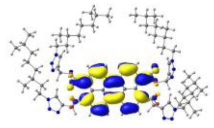	**T_3** **(3.30 eV)**	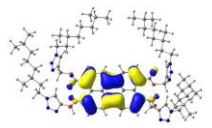	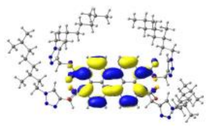
S_2 **(3.99 eV)**	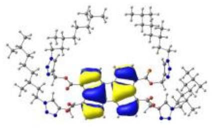	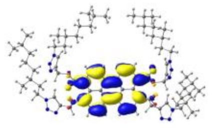	**T_4** **(3.64 eV)**	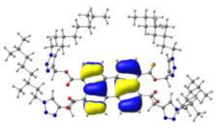	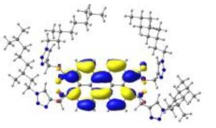
S_3 **(4.18 eV)**	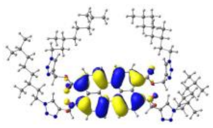	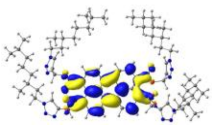	**T_5** **(3.74 eV)**	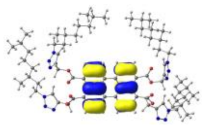	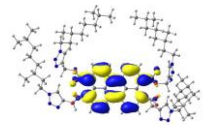
T_1 **(1.79 eV)**	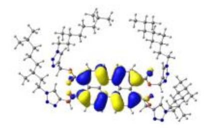	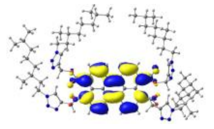	**T_6** **(3.97 eV)**	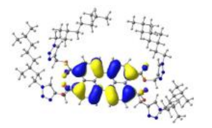	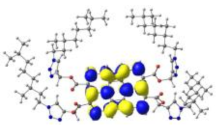
T_2 **(3.19 eV)**	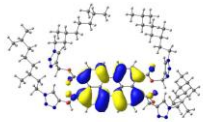	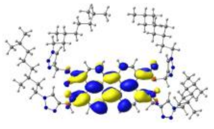	**T_7** **(4.20 eV)**	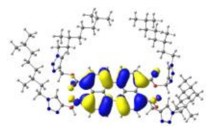	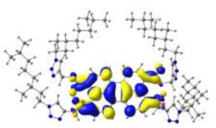

15. Transition density matrix calculation:

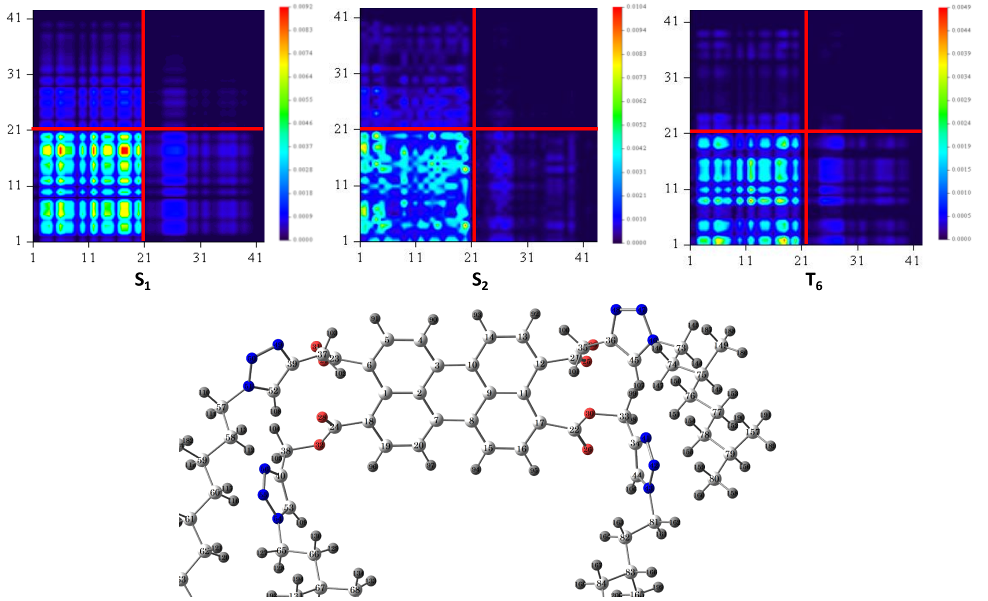

Figure S30. Transition density matrix (TDM) maps of S_1, S_2 and T_6 states of compound **3a** along with chemical structure with atom numbers labelled on it. (Note: We did not show here complete alkyl part as alkyl chains do not contribute to the TDM calculations).

16. Solution-dependent lifetime decay studies:

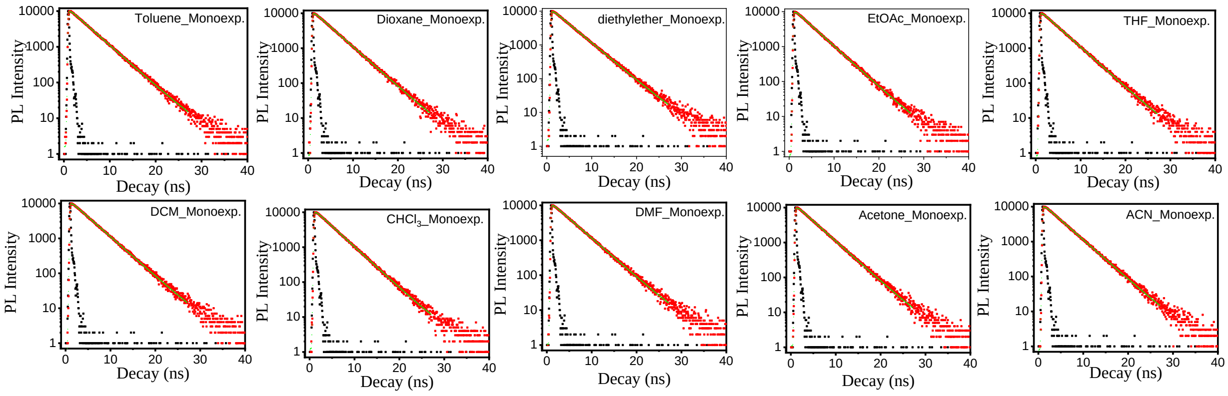

Figure S31. Fluorescence lifetime decay spectra of emitter **3a** in various organic solvents. Prompt IRF shown in Black colored squares; Experimental decay in Red colored squares; Mono-exponential fit in green colored line.

In case of planar molecular structures, triplet-triplet annihilation (TTA) can also be responsible for the high exciton utilization efficiency. In the present case the overall structure of the triazole modified perylene molecules are not exactly planar as can be seen from the optimized structure (compound **3a**) as provided in the Figure S25a. The detailed quantum chemical calculations including natural transition orbitals, singlet-triplet energy levels and transition density matrix calculations for the perylene based emitter **3a** supports the locally excited dominant HLCT character as also reported earlier for the perylene based emitters.[12] In addition, mono-exponential fluorescence decay lifetime (Figure S31) further reinforced our findings.

References:

1. I. Bala, W. Y. Yang, S. P. Gupta, J. De, R. A. K. Yadav, D. P. Singh, D. K. Dubey, J. H. Jou, R. Douali and S. K. Pal, *J. Mater. Chem. C*, 2019, **7**, 5724-5738.
2. I. Bala, S. P. Gupta, S. Kumar, H. Singh, J. De, N. Sharma, K. Kailasam and S. K. Pal, *Soft matter*, 2018, **14**, 6342-6352.
3. J. De, S. P. Gupta, S. S. Swayamprabha, D. K. Dubey, I. Bala, I. Sarkar, G. Dey, J. H. Jou, S. Ghosh and S. K. Pal, *J. Phys. Chem. C*, 2018, **122**, 23659-23674.
4. I. Bala, S. P. Gupta, J. De and S. K. Pal, *Chem. Eur. J.*, 2017, **23**, 12767-12778.
5. S. K. Gupta, S. Setia, S. Sidiq, M. Gupta, S. Kumar and S. K. Pal, *RSC Adv.*, 2013, **3**, 12060-12065.
6. S. G. Alvarez and M. T. A. Alvarez, *Synthesis*, 1997, **4**, 413-414.
7. E. Aydin, B. Nisanci, A. Acar, A. Dastan and Ö. A. Bozdemir, *New J. Chem*, 2015, **39**, 548-554.
8. S. Hirata and M. Head-Gordon, *Chem. Phys. Lett.*, 1999, **314**, 291-299.
9. Grimme, S. *Chem. Phys. Lett.*, 1996, **259**, 128-137.
10. M. Moral, L. Muccioli, W. J. Son, Y. Olivier and J. C. Sancho-Garcia, *J. Chem. Theory Comput.*, 2015, **11**, 168-177.
11. T. Liu, L. Zhu, S. Gong, C. Zhong, G. Xie, E. Mao, J. Fang, D. Ma and C. A. Yang, *Adv. Opt. Mater.*, 2017, **5**, 1700145.
12. Y. Shen, Z. Zhang, H. Liu, Y. Yan, S. Zhang, B. Yang and Y. Ma, *J. Phys. Chem. C*, 2019, **123**, 13047-13056.